Published in final edited form as:
Phys Rev A. 2009 June 18; 79(6): 638271–6382712. doi:10.1103/PhysRevA.79.063827.

Generalized Kramers-Heisenberg expressions for stimulated Raman scattering and two-photon absorption

Oleksiy Roslyak, **Christoph A. Marx**, and **Shaul Mukamel**
Department of Chemistry, University of California, Irvine, California 92697, USA

Abstract

The frequency-domain pump-probe signal of a material system interacting with two quantum modes of the radiation field is recast in terms of products of scattering amplitudes (*T* matrix elements) rather than the third-order susceptibility Im $\chi^{(3)}$. The resulting expression offers a more intuitive physical picture for the optical process compared with the semiclassical approach which treats the radiation field as classical. It can be derived and interpreted using closed-time-path-loop diagrams which represent the joint state of the matter and the field for each contribution to the signal. The signal has two components representing stimulated Raman scattering $\omega_1 - \omega_2$ and two-photon absorption $\omega_1 + \omega_2$ two-photon resonances. Both are expressed as nonequi-librium steady-state photon and matter fluxes, as is common in the description of dissipative processes in open quantum systems.

I. INTRODUCTION

Pump probe spectroscopy is the simplest nonlinear optical technique. The system is subjected to two laser beams: the pump beam with wave vector $\mathbf{k}_1$ and frequency ω_1 and the probe beam ($\mathbf{k}_2$, ω_2). The signal is defined as the change in the transmitted probe beam intensity caused by the pump beam. Apart from single-photon resonances obtained by tuning ω_1 and ω_2 (which can also be observed in linear spectroscopy), the technique also shows new two-photon resonances. Stimulated Raman scattering (SRS) spectroscopy [1–4] focuses on the $\omega_1 - \omega_2$ resonances, whereas the two-photon absorption (TPA) focuses on $\omega_1 + \omega_2$ [5]. Both techniques have been extensively employed since the early days of nonlinear optics. Recent applications include imaging and microscopy [6,7] and femtosecond techniques [8–11].

Nonlinear optical spectroscopy is commonly formulated within the semiclassical (SC) approach whereby a quantum material interacts with classical fields. This convenient theoretical framework has been very successful in the theories of the laser [12] and in describing processes where quantum effects of the fields are negligible [1,13,14]. Most of the current understanding and design of such experiments is based on this language. In an $(n + 1)$-wave mixing process a material sample is exposed to $(n + 1)$ optical fields. Energy exchange between the modes, mediated by the matter-field interaction is observed by monitoring one of these modes, labeled as the signal mode. In spectroscopic applications we extract information about the sample by tuning the fields on-or near-resonance with the material optical transitions. Two detection schemes are commonly used. In heterodyne detection one measures the electric field itself (both amplitude and phase); in homodyne detection the field intensity is measured [14].

Semiclassically, an $(n + 1)$ wave mixing experiment is described as a two-step process. First, the *n* incoming waves induce an *n*th order polarization in the material, which is calculated microscopically by solving the quantum Liouville equation. In a second step, this nonlinear polarization acts as a source in the macroscopic Maxwell equations to generate the signal field. In macroscopic samples the signal field wave vector is given by a linear combination of the incoming pulse wave vectors [1,13–15] and is detected interferrometrically using an external

reference field in the same direction, called the “local oscillator” (LO). This somewhat awkward nomenclature originated in radio wave technology where the receiver is indeed local. The difference in intensity of the LO with and without the signal field defines the heterodyne detected signal:

$$S_{HET}(\mathbf{k}_s,\mathbf{k}_c)\sim N\,\mathrm{Im}\int_{-\infty}^{+\infty}dt\mathscr{E}_s^{\star}(\mathbf{k}_s,t)P_s(\mathbf{k}_c,t). \tag{1}$$

Here, $\mathscr{E}_s(\mathbf{k}_S, t)$ is the complex amplitude of the local oscillator which is assumed to be classical mode propagating in $\mathbf{k}_S$ direction; $P_s(\mathbf{k}_C, t)$ is the polarization induced by a linear combination of incoming modes $\mathbf{k}_C$ and projected on the local oscillator; N is the number of molecules in the sample.

A crucial point in the semiclassical derivation of Eq. (1) is that the local oscillator does not interact with the material sample; it only interferes with the signal field after it has been generated. The pump probe signal can be viewed as self-heterodyne detected where one of the incoming fields (the probe beam) also acts as LO, which, obviously, does interact with the matter in this case and is not spatially separated. Nevertheless the semiclassical theory correctly predicts the SRS and TPA signals, which in the frequency domain are related to the nonlinear susceptibilities.

In this paper we develop an alternative approach for computing frequency domain nonlinear signals by treating both field and matter quantum mechanically. The molecule is viewed as an open system in a nonequilibrium steady state. The signals can be calculated as differences of in and out photon fluxes. In scattering theory fluxes are calculated with the scattering (T) matrix and are given by

$$\sum_{i,f}P_i|T_{fi}|^2\delta(\omega-\omega_{fi}).$$

This Kramers-Heisenberg (KH) (generalized Fermi golden rule) form represents a dissipative process where molecules move between initial $|i\rangle$ and final $|f\rangle$ states at a steady rate. The nature of the process becomes clear and intuitive. The nonlinear susceptibility form (1) while giving the correct signal does not reveal clearly what is really happening to the matter in the course of the process. The T matrix approach is commonly used in statistical mechanisms of open systems such as tunneling junctions or molecular electronics [16,17]. Glauber’s formalism of photon counting is based on transition amplitudes [18]. A rigorous microscopic picture based on scattering amplitudes can have several advantages over the nonlinear susceptibility $\chi^{(3)}$. First, it is highly intuitive and can be used phenomenologically if desired. Second, transition amplitudes are simpler to calculate than susceptibilities. The connection between a scattering and susceptibility picture of linear spectroscopy (Rayleigh scattering) has been the subject of recent interesting debate related to the “sign problem” [19,20]. The present work establishes this connection for nonlinear signals. We show how heterodyne-detected signals can be recast in the generalized KH form and demonstrate its equivalence to the standard nonlinear susceptibility $\chi^{(3)}$ approach.

In the following two sections we present two essential ingredients of the formalism that will be used to accomplish our goal. In Sec. II we formulate the nonlinear wave mixing using a quantum description of the fields and matter [21]. This establishes unified description of heterodyne and self-heterodyne detected signals. The local oscillator needs not to be spatially separated from the material. All modes, including the detected mode, interact with the sample. The signal mode is singled out only by the fact that it is detected but not by the way it interacts

with the system. We assume that all modes, including the detected mode, are initially in a coherent state. The change in the mode intensity is driven by the nonlinear polarization of individual molecules induced by the incoming modes. The molecules are uncorrelated and give rise to the incoherent response from the sample that scales linearly with the number of molecules *N*. Unlike the SC approach, the Maxwell equations and macroscopic propagation effects are not needed for defining the signal. We can simply consider the response of a single molecule and multiply it by *N*. This will be helpful for microscopy applications which involve a single or a few molecules.

In Sec. III we present a closed-time-path-loop (CTPL) representation of heterodyne-detected signals. Time domain (TD) nonlinear signals are usually described by the density matrix and represented by double-sided Feynman diagrams [14]. These keep track of the relative time ordering of the various interactions by working in the Liouville space (following the bra and the ket simultaneously). The loop diagrams are only partially time ordered and provide a picture in the Hilbert space where the ket by moves forward and backward in time [22,23]. The CTPL formalism is most natural for frequency-domain techniques where time ordering is not maintained anyhow [21,24]. The rules for constructing and reading loop diagrams are explained.

In Sec. IV, using the nonequilibrium steady-state approach solely based on photon fluxes, we derive the closed KH expressions for the stimulated Raman scattering and the two-photon absorption signals in terms of absolute squares of scattering amplitudes [transition amplitude (TA)]. The loop lends itself directly for the derivation of KH expressions. By dissecting the loop into its forward and backward branches we obtain the *T* matrix elements. Using the transformation rules for the loop diagrams, in Sec. V we obtain the KH forms of the two-photon absorption and stimulated Raman scattering from $\chi^{(3)}$. This establishes connection between the CTPL and TA approaches. Both approaches yield the same result but offer different interpretations. Section VI summarizes our results.

II. HETERODYNE DETECTION AS A STIMULATED PROCESS: QUANTUM FIELD FORMULATION

A material sample interacting with a quantized electric field is described by the Hamiltonian

$$H(t)=H_0+H_{int}(t), \tag{2}$$

where H_0 represents the bare material system and $\hat{H}_{int}(t)$ is the matter-field interaction. Equation (2) is written in the interaction picture with respect to the field where the field Hamiltonian is eliminated. We work in the units where $\hbar = 1$.

The coupling between the material and the field is mediated by the dipole operator, $V(\mathbf{r}) + V^{\dagger}(\mathbf{r})$. Here the first term is the positive frequency (de-excitation) part defined by

$$V(\mathbf{r})=\sum_{\alpha=1}^{N}\delta(\mathbf{r}-\mathbf{r}_{\alpha})\sum_{j}\sum_{k>j}\mu_{jk}|j\rangle\langle k|, \tag{3}$$

where $\{|k\rangle\}$ represent the eigenstates of the bare material system labeled according to increasing energy.

Similarly the field is partitioned as $E(\mathbf{r}, t) + E^{\dagger}(\mathbf{r}, t)$, where the field annihilation operator at $\mathbf{r}$ and time *t* is given by

$$E(\mathbf{r},t)=\sum_{j=1}^{n+1}\left(\frac{2\pi\omega_j}{\Omega}\right)^{1/2} a_j e^{i(\mathbf{k}_j\mathbf{r}-\omega_j t)}. \tag{4}$$

Here, a_j ($a_j^\dagger$) are the annihilation (creation) operators for the jth field mode, satisfying the bosonic commutation relation $[a_j, a_{j'}^\dagger]=\delta_{jj'}$. The index "$j$" runs over all the relevant field modes and Ω is the quantization volume.

In the rotating wave approximation (RWA), $H_{int}(t)$ assumes the form

$$H_{int}(t)=E(\mathbf{r},t)\,V^\dagger+E^\dagger(\mathbf{r},t)\,V. \tag{5}$$

The (n + 1)th mode is singled out by the detection. Its electric field operator consists of two terms: $E_{n+1}(\mathbf{r}, t) = \mathcal{E}_s(\mathbf{r}, t) + E_s(\mathbf{r}, t)$. The classical (coherent) part $\mathcal{E}_s(\mathbf{r}, t) = \mathcal{E}_s \exp[i(\mathbf{k}_s)\mathbf{r} - \omega_s t]$ is not affected by the interactions with the molecules. The second term $E_s(\mathbf{r}, t)$ is initially in the vacuum state and populated due to the coupling with the material. The signal is defined as the change in the intensity of the detected mode due to the remaining n incoming modes. In other words, we measure the change in the detected mode intensity with and without the material sample:

$$\begin{aligned} S(t) &= \frac{1}{\mathcal{E}_s^\star(\mathbf{r},t)\mathcal{E}_s(\mathbf{r},t)}\left\{\int d\mathbf{r}\left\langle[\mathcal{E}_s^\star(\mathbf{r},t)+E_s^\dagger(\mathbf{r},t)]\times[\mathcal{E}_s(\mathbf{r},t)+E_s(\mathbf{r},t)]\right\rangle-\mathcal{E}_s^\star(\mathbf{r},t)\mathcal{E}_s(\mathbf{r},t)\right\} \\ &= \frac{\Omega}{2\pi\omega_s}\left[2\Re\int d\mathbf{r}\,\langle\mathcal{E}_s^\star(\mathbf{r},t)E_s(\mathbf{r},t)\rangle+\int d\mathbf{r}\left\langle E_s^\dagger E_s(\mathbf{r},t)\right\rangle\right]. \end{aligned} \tag{6}$$

The self-heterodyne part of the signal [Eq. (6)] is given by the first term. This term dominates the signal since usually $\mathcal{E}_s^\star\mathcal{E}_s \gg \langle E_s^\dagger E_s\rangle$. The expectation value of the induced electric field can be calculated using the Heisenberg equation of motion for the detected mode:

$$\begin{aligned} \frac{d}{dt}\langle\mathcal{E}_s^\star(\mathbf{r},t)E_s(\mathbf{r},t)\rangle &= i\mathcal{E}_s^\star(\mathbf{r},t)\langle[H_{int},E_s(\mathbf{r},t)]\rangle \\ &= i\mathcal{E}_s^\star(\mathbf{r},t)\left(\frac{2\pi\omega_s}{\Omega}\right)\langle V(\mathbf{r},t)\rangle\, e^{-i\mathbf{k}_s\mathbf{r}}. \end{aligned} \tag{7}$$

Here we took into account that the $\mathcal{E}_s^\star(\mathbf{r}, t)$ part of the detected mode is not affected by the interaction with the matter $\left[H_{int}, \mathcal{E}_s^\star(\mathbf{r}, t)\right]=0$. We also introduced the averaging over the coupled light and matter $\langle V(\mathbf{r}, t)\rangle$ = Tr[V(**r**)ρ(t)] described by the time-dependent density operator ρ(t). The solution of this equation along with the initial condition $\langle E_s(\mathbf{r}, t = -\infty)\rangle = 0$ can be substituted into Eq. (6), which yields for the stationary self-heterodyne signal:

$$S_{HET}=2\,\mathrm{Im}\int d\mathbf{r}e^{-i\mathbf{k}_s\mathbf{r}}\int_{-\infty}^{\infty}dt\mathcal{E}_s^\star(t)\langle V(\mathbf{r},t)\rangle. \tag{8}$$

Expanding ρ(t) to first order in each of the n incoming modes and summing over all the molecules in the sample, we obtain $\langle V(\mathbf{r}, t)\rangle$ in the terms of the nonlinear polarization $P_c(t)$ calculated in the $\mathbf{k}_c=\sum_{i=1}^{n}\pm\mathbf{k}_i$ direction:

$$\langle V(\mathbf{r},t)\rangle = \sum_{\alpha=1}^{N} \delta(\mathbf{r}-\mathbf{r}_\alpha) P_c(t) e^{i\mathbf{k}_c\mathbf{r}}. \tag{9}$$

The heterodyne detected (n + 1) wave mixing signals are thus directed along one of the 2^n directions given by all possible plus minus combinations of the n incoming wave vectors. Substituting Eq. (9) into Eq. (8) we obtain the signal as

$$S_{HET} = 2N \,\mathrm{Im} \int_{-\infty}^{+\infty} dt \mathscr{E}_s^{\star}(t) P_c(t), \tag{10}$$

where we assumed the sample to be large enough for the perfect phase matching $\mathbf{k}_s - \mathbf{k}_c = 0$.

Comparing Eq. (10) with Eq. (1) we conclude that there is no principal difference between ordinary and self-heterodyne detected signals. The following microscopic interpretation of heterodyne-detected signals is offered by Eq. (10): all n + 1 fields (including LO) interact with the matter and all n + 1 transitions are *stimulated*. We measure the change in intensity of the local oscillator. For a large sample, a change in its intensity will occur only if $\mathbf{k}_s$ approximately coincides with one of the directions $\mathbf{k}_c$ or equivalently $\omega_c - \omega_s = 0$. The nonlinear polarization induced by n incoming modes contains all the information necessary to calculate the signal.

III. DIAGRAMMATIC CLOSED-TIME-PATH-LOOP CALCULATION OF HETERODYNE SIGNALS

Equation (10) serves as a convenient starting point for calculating nonlinear optical signals. The nonlinear optical polarization $P_c(t)$ with a given wave vector $\mathbf{k}_c$ will be calculated using a perturbative expansion of the density operator $\rho(t)$ with respect to the incoming n modes. In this section we show how this expansion may be performed diagrammatically using the CTPL. The loop expansion may be formulated either in the time or frequency domain. Here we shall focus on the frequency domain formation. However, since the time-domain formulation is closely related to double-sided Feynman diagrams, we present both. The rules for constructing and reading time- and frequency-domain diagrams are summarized in Appendixes A and B, respectively.

In the SC theory, optical signals are given by causal response functions of the material to the classical field [14]. In a quantum treatment of the field these are replaced by products of matter and field superoperator nonequilibrium Green's functions (SNGFs) [17] which represent the response as well as spontaneous fluctuations in both matter *and* field. The CTPLs provide an intuitive diagrammatic approach for computing the SNGF.

In the time domain, the loop is understood as a diagrammatic representation of the density operator. This interpretation relies on its perturbative Liouville space expansion in the incoming modes. We associate with each Hilbert-space operator A, a left (L) and a right (R) superoperators [25,26]:

$$\begin{aligned} A_L X &= AX, \\ A_R X &= XA, \end{aligned} \tag{11}$$

where X denotes an arbitrary operator. We further introduce the density operator in the L / R representation:

$$\rho(t)=\exp\left\{-i\int_{-\infty}^{t}[H_{int,L}(\tau)-H_{int,R}(\tau)]d\tau\right\}\rho(-\infty). \tag{12}$$

Perturbative expansion of the density operator [Eq. (12)] to first order in each of the incoming *n* modes yields the time-domain signal [Eq. (10)] in terms of the matter SNGF times the field SNGF. Each SNGF is a partially time-ordered correlation function of the dipole or the field *L* / *R* superoperators. Partial time ordering means time ordering for *L* and *R* superoperators, but there is no time ordering between those groups of the superoperators. The time dependence of the dipole superoperators stems from the transformation to the interaction picture with respect to the bare molecule:

$$V_{\nu}(t)=\exp[\,i(H_{0,L}-H_{0,R})t]V_{\nu}\exp[\,-i(H_{0,L}-H_{0,R})t], \tag{13}$$

where the subscript ν stands either for *L* or *R* superoperator.

The CTPLs provide a graphic representations of the SNGFs. The left branch describes $V_L(t)$ $E_L(t)$ interaction, and the right branch shows $V_R(t)E_R(t)$ interactions. The loop diagrams are *partially* time ordered in contrast to the *fully* time-ordered double-sided Feynman diagrams. The latter are pictorial representation of the perturbative expansion of the density operator in the Liouville space,

$$\rho(t)=\exp\left[-i\int_{-\infty}^{t}\Omega_{int}(\tau)d\tau\right]\rho(-\infty). \tag{14}$$

The left branch describes the ket and the right the bra. Since for the CTPL interactions on the left and the right branches are not time-ordered *relative* to each other [rule (TD6), Appendix A], it gives a more compact representation [(*n* + 1) terms] than the double-sided Feynman diagrams (2^n terms) for the *n*th-order response. Double-sided Feynman diagrams can be generated from the CTPL diagrams by keeping track of the relative time ordering between interactions occurring with the ket and the bra [rule (TD6), Appendix A]. Therefore the CTPL's present no advantage over the double-sided Feynman diagrams for a time domain experiment with non-overlapping optical pulses where all interaction times are controlled. In the frequency domain the time ordering between the interactions is not maintained, and the loop diagrams provide a compact picture in the Hilbert space where the ket evolves forward (left branch) and then backward in time (across the loop and on the right branch).

The loop represents a state vector in the Hilbert space, propagated clockwise along a closed time pathway between $-\infty$ and the observation time *t*, i.e., $-\infty \rightarrow t \rightarrow -\infty$. CTPLs were originally introduced in quantum field theory to describe nonequilibrium states [27–31]. The following two points are crucial for distinguishing the CTPL from the double-sided Feynman diagrams. First, in the density-matrix approach one may look at the ket and the bra separately when drawing the diagrams for particular processes. The construction is then done starting at the bottom of each branch and ending at its top, making sure that the material system is in a diagonal element of the density operator at the observation time *t* (otherwise the trace vanishes). We can therefore think of the process as forward propagation in time on both the ket and bra. The second point concerns the last interaction which can act on either the left or the right branch since this leaves the corresponding matter-SNGF invariant $\{\mathrm{Tr}[V\rho(t)] = \mathrm{Tr}[\rho(t)V]\}$. We adopt the convention that the last interaction occurs from the left [rule (TD5) in Appendix A]. However, this choice does affect the physical interpretation of each interaction as either absorption or emission. This is an ambiguity intrinsic to double-sided Feynman diagrams. In

the CTPL this is resolved at the price of having to introduce backward propagation on the right branch of the loop diagram.

Using rule (FD8) in Appendix B we define the retarded Hilbert-space propagator

$$G(\omega)=\frac{1}{\omega - H_0+i\gamma}. \tag{15}$$

The infinitesimal $\gamma > 0$ arises from causality and guarantees the convergence of the Fourier transform.

There are two basic transformations of loop diagrams. Changing the last interaction from the top left to the top right leaves a diagram, i.e., its corresponding SNGF, invariant. Similarly, a reflection of all interactions through the center line between the two branches amounts to taking the complex conjugate of the related SNGF. This follows from $\langle AB\cdots Z\rangle^{\star} = \langle Z^{\dagger}\cdots B^{\dagger}A^{\dagger}\rangle$.

In summary, in the frequency domain, the loop representation has several advantages and resolves some conceptual ambiguities that arise in the double-sided Feynman diagrams. One associates forward propagation with the left and backward propagations with the right branch of the loop. This implies that an arrow pointing to the right (left) always represents absorption (emission) regardless on whether it occurs with the left or the right branch. In particular, changing the last interaction from the left to the right branch consequently does not change its physical meaning. Hence for a given frequency-domain diagram, there is no ambiguity about the absorption or emission nature of the interaction at the observation time. Ambiguity does exist in the density-matrix representation which involves all-forward propagation and connects better to time-domain experiments.

In a coherent parametric process the signal frequency is given by a combination of the other field frequencies. We now apply the CTPL to compute the four wave mixing signal at $\mathbf{k}_c = -\mathbf{k}_1 + \mathbf{k}_2 + \mathbf{k}_3$. Pump probe spectroscopy is a special case of this signal, as will be demonstrated in the coming sections. Applying rule (FD3), we find that in this technique fields $\mathbf{k}_2$ and $\mathbf{k}_3$ are absorbed, (and represented by arrows pointing to the right) whereas $\mathbf{k}_1$ and $\mathbf{k}_s$ are emitted (arrows pointing to the left). The diagrams are generated by considering all possible ways of distributing these arrows along the loop under the constraint that the interaction with $\mathbf{k}_s$ is fixed to the top left branch. We illustrate this for a three-level ladder model system with sequential ($|g\rangle \rightarrow |e\rangle$ and $|e\rangle \rightarrow |f\rangle$) dipole coupling, as shown in Fig. 1.

In accordance with the energy conservation in the field, the loop describes propagation along the closed time path $-\infty \rightarrow t \rightarrow -\infty$, where the material system must start and end in the ground state $|g\rangle$. Within the RWA this implies that along the loop the first interaction must be an absorption and the last an emission. This gives the eight diagrams shown in Fig. 2.

We adopt the following convention for the Fourier transform:

$$\begin{aligned} A(\tau)&=\tfrac{1}{2\pi}\int d\omega A(\omega)e^{-i\omega\tau} \\ A(\omega)&=\int d\tau A(\tau)e^{i\omega\tau}. \end{aligned} \tag{16}$$

We next use frequency-domain rules to calculate the heterodyne signal at $\mathbf{k}_c$. We note that the loop diagrams can be naturally divided into two groups. The first group given by (a)–(d) in Fig. 2 involves the sequence $V^{\dagger}V^{\dagger}VV$, i.e., photon absorption, absorption, emission, and emission. It should be emphasized that this order along the loop does not represent an ordering in real time. All two-photon resonances of the type $\omega_i + \omega_j$ are included in this group, we thus

label it TPA. The second group given by pathways (e)–(h) in Fig. 2 represents the sequence $V^{\dagger}VV^{\dagger}V$, i.e., photon absorption, emission, absorption, and emission; which correspond to SRS resonances of the form $\omega_i - \omega_j$. Using the loop diagram rules in Appendix B we get two contributions to the heterodyne-detected signal:

$$S_{HET} = -4\pi N\delta(\omega_s - (-\omega_1+\omega_2+\omega_3)) \times \Im \mathscr{E}_s^{\star}\mathscr{E}_1^{\star}\mathscr{E}_2\mathscr{E}_3\chi^{(3)}(-\omega_s;\omega_3,\omega_2,-\omega_1) \tag{17}$$

Here the third-order susceptibility is partitioned into its two-photon absorption and stimulated Raman scattering parts $\chi^{(3)}=\chi^{(3)}_{TPA}+\chi^{(3)}_{SRS}$ as

$$\chi^{(3)}_{TPA}(-\omega_s;\omega_3,\omega_2,-\omega_1)=\left[\left\langle VG(\omega_2+\omega_3-\omega_1+\omega_g)VG(\omega_2+\omega_3+\omega_g)\times V^{\dagger}G(\omega_2+\omega_g)V^{\dagger}\right\rangle+\left\langle VG(\omega_3+\omega_2-\omega_1+\omega_g)\times VG(\omega_3+\omega_2+\omega_g)V^{\dagger}G(\omega_3+\omega_g)V^{\dagger}\right\rangle+\left\langle VG^{\dagger}(\omega_2+\omega_3-\right.\right. \tag{18}$$

$$\chi^{(3)}_{SRS}(-\omega_s;\omega_3,\omega_2,-\omega_1)=\left[\left\langle VG(\omega_2-\omega_1+\omega_3+\omega_g)V^{\dagger}G(\omega_2-\omega_1+\omega_g)\times VG(\omega_2+\omega_g)V^{\dagger}\right\rangle+\left\langle VG(\omega_3-\omega_1+\omega_2+\omega_g)\times V^{\dagger}G(\omega_3-\omega_1+\omega_g)VG(\omega_3+\omega_g)V^{\dagger}\right\rangle+\left\langle VG^{\dagger}(\omega_2-\omega_s\right.\right. \tag{19}$$

Note that the momentum conservation condition could have also been multiplied by (−1), thereby reversing all signs of the wave vectors. All absorptions then become emissions and vice versa. Diagrammatically this can be achieved by a reflection of all interactions through the center line between the left and right branches. This transformation corresponds to taking the complex conjugate of the associated SNGF. Since the signal is proportional to the imaginary part of the polarization [$\mathrm{Im}(z^{*}) = -\mathrm{Im}(z)$], this operation will cause an overall change in sign. This sign change simply implies that *all* the interactions (absorptions and emissions) have been reversed in their physical interpretation.

We may hence interpret the process either as an emission ($-\mathbf{k}_s + \mathbf{k}_c = 0$) or an absorption ($\mathbf{k}_s - \mathbf{k}_c = 0$) of a photon in the detected mode. This freedom arises because the field is assumed to be in a coherent state which is given by the following superposition of number states $|n\rangle$:

$$\begin{aligned} |\Psi_c &= \exp\left(-\sum_j |\alpha_j|^2\right)\exp\{\alpha a^{\dagger}\}|0 \\ &= \exp\left(-\sum_j |\alpha_j|^2\right)\sum_{n=0}^{\infty}\frac{\alpha}{\sqrt{n!}}|n. \end{aligned} \tag{20}$$

Here, $|0\rangle$ is the vacuum state.

A coherent state is an eigenstate of the annihilation operator,

$$a|\Psi_C\rangle=\alpha|\Psi_C\rangle \quad \text{and} \quad \langle\Psi_C|a^\dagger a|\Psi\rangle=|\alpha|^2. \tag{21}$$

Therefore for a coherent state adding or removing one photon does not change the average number of photons.

The quantum description of the fields suggests a natural classification of $(n + 1)$-wave mixing experiments as either phase sensitive or phase insensitive. A nondegenerate $(n + 1)$-wave mixing signal performed with $(n + 1)$ different modes each initially in a number state is not possible since its amplitude vanishes identically. However, degenerate processes whereby each creation operator is accompanied by the corresponding annihilation operator give a nonvanishing field correlation function. Macroscopically, such phase-insensitive signals involve exact phase cancellation of the fields. These experiments can be readily interpreted in terms of photon occupation numbers. Since phase-insensitive signals are possible for optical Fock states, they can be derived alternatively using transition amplitudes represented by single-sided Feynman diagrams. In doing so, it will be possible to partition the diagrams into absorptions and emissions of a photon in the detected mode. This picture will be used in the next two sections where we first derive the pump probe signal in terms of photon fluxes in a nonequilibrium steady state (Sec. IV) and then show how the CTPL expression can be recast in the same form by dissecting the diagrams along their center lines (Sec. V).

IV. PUMP-PROBE SIGNAL EXPRESSED AS A NONEQUILIBRIUM STEADY-STATE PHOTON AND MATTER FLUX

This section provides an intuitive derivation of the pump-probe signal using scattering amplitudes without resorting to susceptibilities. Single-sided diagrams represent transition amplitudes corresponding to the system undergoing a change from a given initial (matter/field) state to a specified final state. Only forward propagation is necessary which allows for a more intuitive picture. This is however only possible for phase-insensitive processes, described in terms of number states of the field.

The pump probe technique is a self-heterodyne detected stimulated process. It involves two beams with wave vectors $\mathbf{k}_1$ and $\mathbf{k}_2$. In general the beams may also differ in their polarization direction. Polarization indices are omitted here for clarity. The intensity of one of the two modes ($\mathbf{k}_2 = \mathbf{k}_s$ as the probe beam) is monitored, whereas the other mode ($\mathbf{k}_1$) is referred to as the pump beam. The signal is defined as the difference in the transmitted intensity of the probe beam, with and without the pump beam [Eq. (8)].

To calculate this signal we note its independence on the phases of the fields. In a quantum description of the field this implies that each field creation operator must be accompanied by the corresponding annihilation operator. The process may therefore be described in terms of a Fock state for the field. Let $|n_1, n_2\rangle$ denote the initial state of the two modes at $t \to -\infty$. In order for a pathway to contribute to the signal at t, the number of photons of the probe beam (n_2) must change. By definition, the signal represents how this change is mediated by the pump beam. We only consider the lowest-order processes where the number of photons in each mode may change by ±1 at most. The matter is described by the three-band model system shown in Fig. 1.

The possible processes may be classified according to the net change in the number of photons in the probe beam between $-\infty$ and observation time t. To lowest order in the probe beam, the effect can either be photon emission ($n_2 \to n_2 + 1$) or absorption ($n_2 \to n_2 - 1$). In each case the number of photons of the pump beam may have either changed ($n_1 \to n_1 \pm 1$) or returned

to its initial value ($n_1 \rightarrow n_1$). In total, this gives rise to six processes in the joint two-mode space. However only three survive the RWA. We show this diagrammatically. First, we note that when going around the loop, the joint matter-field system must start and end in the same state $|n_1, n_2\rangle$. Since at time t the number of photons in the probe beam must change, to lowest order, the system has to undergo one interaction with the probe beam on either side of the loop. Overall phase cancelation then requires two additional interactions with the pump beam. Formally the signal will therefore be given in terms of four-point correlation functions (two interactions with the pump beam and two with the probe beam).

Applying these rules to each of the six possible processes with a total of four interactions, the processes $|n_1, n_2\rangle \rightarrow |n_1 + 1, n_2 + 1\rangle$, $|n_1, n_2\rangle \rightarrow |n_1, n_2 + 1\rangle$, and $|n_1, n_2\rangle \rightarrow |n_1 + 1, n_2 - 1\rangle$ shown in Fig. 3 do not contribute within the RWA and may be neglected. All three diagrams involve de-exciting the molecule from its ground state.

The eight contributing loop diagrams are shown in Fig. 5. Each diagram can be associated with one of the four possible processes: (i) $|n_1, n_2\rangle \rightarrow |n_1 - 1, n_2 + 1\rangle$, (ii) $|n_1, n_2\rangle \rightarrow |n_1 - 1, n_2 - 1\rangle$, (iii) $|n_1, n_2\rangle \rightarrow |n_1, n_2 - 1\rangle$, and (iv) $|n_1, n_2\rangle \rightarrow |n_1 + 1, n_2 - 1\rangle$. Due to phase cancelation of the fields, they only enter in form of modulus squares (intensities). This allows them to be taken out of the imaginary part of Eq. (10); what remains is the imaginary part of the matter correlation functions.

Figure 4 gives the single-sided diagrams for each of the four processes (i)–(iv). In contrast to the loop, time now goes forward from bottom to top. Different pathways may interfere in a given process. The total amplitude of each process is hence given as the sum of the amplitudes of the possible pathways. The material transition amplitudes are given in Appendix C. Since the fields are in coherent states, their transition amplitudes are simply given by products of corresponding electrical fields of the modes, as in the SC theory.

Processes (i) and (iv) are each given by single two-photon TA for the matter and light interacting system,

$$T_i = \mathscr{E}_1 \mathscr{E}_2 \mathscr{T}^{(2)}_{g'g}(\omega_1), \tag{22}$$

$$T_{iv} = \mathscr{E}_1 \mathscr{E}_2 \mathscr{T}^{(2)}_{g'g}(\omega_2). \tag{23}$$

Process (ii) are given by two two-photon TA,

$$T_{ii} = \mathscr{E}_1 \mathscr{E}_2 [\, \mathscr{T}^{(2)}_{fg}(\omega_1) + \mathscr{T}^{(2)}_{fg}(\omega_2)]. \tag{24}$$

There are five TA (one single-photon and four three-photon) for process (iii):

$$T_{iii} = \mathscr{E}_2 \mathscr{T}^{(1)}_{eg} + \mathscr{E}_2 |\mathscr{E}_1|^2 [\, \mathscr{T}^{(3)}_{eg}(\omega_1 - \omega_1, \omega_1) + \mathscr{T}^{(3)}_{eg}(\omega_2 + \omega_1, \omega_2) + \mathscr{T}^{(3)}_{eg}(\omega_1 + \omega_2, \omega_1) + \mathscr{T}^{(3)}_{eg}(\omega_2 - \omega_1, \omega_2)]. \tag{25}$$

All material $\mathscr{T}$ matrix elements are given in Appendix C. The pump-probe signal is given by the absolute square of the amplitudes of each process scaled with corresponding resonant factor (Dirac delta function). The signal can be interpreted as the difference between stimulated

emission (positive) and absorption (negative) in the detected mode (probe beam in this paper). This gives us Kramers-Heisenberg form (indicated by the tilde) of the pump-probe signal,

$$\tilde{S}_{PP}(\omega_1,\omega_2)=4\pi N\sum_{g,g',e,f}P(g)[\,|T_i|^2\delta(\omega_1-\omega_2-\omega_{g'g})-|T_{iv}|^2\delta(\omega_2-\omega_1-\omega_{g'g})-|T_{ii}|^2\delta(\omega_1+\omega_2-\omega_{fg})-|T_{iii}|^2\delta(\omega_2-\omega_{eg})].$$

(26)

Here $P(g)$ is the equilibrium population of the ground state $|g\rangle$. T_i represents an overall gain of photons in the detected mode (stimulated emission), whereas T_{ii}, T_{iii}, and T_{iv} represent loss (absorption). The first two terms represent SRS as a difference of two photon fluxes. The third term represents TPA as a two-photon flux. When the photon frequencies are tuned off any single-photon resonance, the last term vanishes. Otherwise it provides a resonant contribution to the signal. From Eq. (26) we see that it contains both SRS- and TPA-type resonances. Note that in order to get the Kramers-Heisenberg form we had to include terms with different orders in the fields $\sim\mathcal{E}^2$ and $\sim\mathcal{E}^6$. The actual pump-probe signal is obtained from Eq. (26) by keeping only the contributions which scale as $\sim|\mathcal{E}_1|^2|\mathcal{E}_2|^2$.

Notice that the only ingredient necessary to derive Eq. (26) is the changes in the number of photons in the optical modes. Since we monitor the change in the probe beam mode only Δn_2 defines the sign of each term. In the next section we show how this result can be derived using the CTPL expansion of $\chi^{(3)}$.

V. PUMP-PROBE SPECTROSCOPY REVISITED: FACTORIZING $\chi^{(3)}$ INTO TRANSITION AMPLITUDES

The pump-probe signal can be obtained from Eqs. (18) and (19) as in self-heterodyne detections by putting $\mathbf{k}_3 = \mathbf{k}_1$ and $\mathbf{k}_s = \mathbf{k}_1$. It is given by $\chi^{(3)}(-\omega_2; \omega_2, -\omega_1, \omega_1)$.

We start with the loop diagrams for the pump probe signal shown in Fig. 5. The material correlation functions representing the diagrams may be recast in the form products of amplitudes corresponding to single-sided Feynman diagrams. To this end we consider each branch of the loop separately. Pictorially this amounts to dissecting the loop along its center line. Such dissection is possible, since by definition, the top of both branches represents the matter-field system at the same time t. Formally this can be obtained by inserting the identity after the dipole operator representing the interaction at t. Applying rules (FD7)–(FD9) in Appendix A, the advanced propagator $G^{\dagger}(\Delta\omega + \omega_g)$ joins the two branches as shown in Fig. 6. Here, $\Delta\omega$ denotes the cumulative sum of the signed field frequencies of the interactions on the left branch. Physically, $\Delta\omega$ represents the change in the energy of the field that has occurred between $-\infty$ and t. Each branch is treated separately and represents a scattering amplitude which may be represented by a single-sided Feynman diagram.

The signal has two components: two-photon absorption and stimulated Raman scattering,

$$S_{PP}(\omega_1,\omega_2)=S_{TPA}(\omega_1,\omega_2)+S_{SRS}(\omega_1,\omega_2). \quad (27)$$

Using the definitions in Appendix C the two-photon absorption contribution can be written in terms of the complex amplitudes as

$$S_{TPA}(\omega_1,\omega_2) = -4\pi N|\mathscr{E}_1|^2|\mathscr{E}_2|^2\,\mathrm{Im}\sum_{g,e,f}P(g)[\,|\mathscr{T}^{(2)}_{fg}(\omega_1)|^2+\mathscr{T}^{(2)}_{fg}(\omega_1)\mathscr{T}^{(2),\star}_{fg}(\omega_2)]\frac{1}{\omega_2+\omega_1-\omega_{fg}-i\gamma}$$
$$+P(g)[\,\mathscr{T}^{(1)}_{eg}\mathscr{T}^{(3),\star}_{eg}(\omega_2+\omega_1,\omega_2)+\mathscr{T}^{(1)}_{eg}\mathscr{T}^{(3),\star}_{eg}\times(\omega_1+\omega_2,\omega_1)]\frac{1}{\omega_2-\omega_{eg}-i\gamma}. \quad (28)$$

The first term corresponds to diagrams (a) and (b) in Fig. 5, the second term is related to diagrams (f) and (g).

Similarly the stimulated-Raman scattering signal can be written as

$$S_{SRS}(\omega_1,\omega_2) = 4\pi N|\mathscr{E}_1|^2|\mathscr{E}_2|^2 \times \mathrm{Im}\sum_{g,g',e}|\mathscr{T}^{(2)}_{g'g}(\omega_1)|^2\frac{1}{\omega_1-\omega_2-\omega_{g'g}-i\gamma} - P(g)[\,\mathscr{T}^{(1)}_{eg}\mathscr{T}^{(3),\star}_{eg}(\omega_1-\omega_1,\omega_1)+\mathscr{T}^{(1)}_{eg}\mathscr{T}^{(3),\star}_{eg}(\omega_2-\omega_1,\omega_2)+\mathscr{T}^{(3)}_{eg}(\omega_1-\omega_1,\omega_1)\mathscr{T}^{(1),\star}_{eg}]\times\frac{1}{\omega_2-\omega_{eg}-i\gamma}. \quad (29)$$

The first term corresponds to diagram (h) in Fig. 5, the second term is related to diagrams (c)–(e).

In these equations we have expressed $\chi^{(3)}$ in terms of products of T matrix elements. This is a step toward recasting the signal in the KH form of Eq. (26). Note that Eq. (27) unlike Eq. (26) does not contain the matrix elements which correspond to the pump beam being the last to interact with the matter. These terms are the only difference between those equations provided one neglects the high-order terms (to fourth order in the field). As we show below these terms mutually cancel each other. We prove the statement by adding and subtracting diagrams with the last interaction occurring with the pump beam instead of the probe beam from the signal [Eq. (27)].

We start with the SRS part of the pump probe signal. Let us consider diagram (h) in Fig. 5 and interchange the pump beam and the probe beam so that the last interaction occur with the pump beam. Using the basic transformation rules of Sec. III (the last interaction is brought to the right branches and then the diagrams are reflected with respect to the central line) one can prove the following identity:

$$4\pi N\,\mathrm{Im}\sum_{g,g',e,f}P(g)|\mathscr{E}_2|^2|\mathscr{E}_1|^2\times\left[\mathscr{T}^{(3)}_{eg}(\omega_2-\omega_1,\omega_2)\mathscr{T}^{(1),\star}_{eg}\frac{1}{\omega_2-\omega_{eg}-i\gamma}+|\mathscr{T}^{(2)}_{g'g}(\omega_2)|^2\frac{1}{\omega_2-\omega_1-\omega_{g'g}-i\gamma}\right]=0. \quad (30)$$

Here the first term corresponds to the pump beam absorption, and the second term stands for the pump beam emission, and the total contribution from this terms is zero. We will also need the following trivial identity:

$$4\pi N \,\mathrm{Im} \sum_{g,g',e,f} P(g)[\,\mathscr{T}_{eg}^{(1)}|\mathscr{E}_2|^2 - \mathscr{T}_{eg}^{(1)}|\mathscr{E}_2|^2]\frac{1}{\omega_2 - \omega_{eg} - i\gamma} = 0 \tag{31}$$

and the high-order terms

$$\begin{aligned} 4\pi N \,\mathrm{Im} \sum_{g,g',e,f} & P(g)|\mathscr{E}_1|^4|\mathscr{E}_2|^2 \frac{1}{\omega_2 - \omega_{eg} - i\gamma} \\ & \times [\,\mathscr{T}_{eg}^{(3)}(\omega_2 \\ & - \omega_1, \omega_2)\mathscr{T}_{eg}^{(3),\star}(\omega_2 \\ & - \omega_1, \omega_2) + \mathscr{T}_{eg}^{(3)}(\omega_1 \\ & - \omega_1, \omega_1)\mathscr{T}_{eg}^{(3),\star}(\omega_1 \\ & - \omega_1, \omega_1) + \mathscr{T}_{eg}^{(3)}(\omega_2 \\ & - \omega_1, \omega_2)\mathscr{T}_{eg}^{(3),\star}(\omega_1 \\ & - \omega_1, \omega_1) + \mathscr{T}_{eg}^{(3)}(\omega_1 \\ & - \omega_1, \omega_1)\mathscr{T}_{eg}^{(3),\star}(\omega_2 \\ & - \omega_1, \omega_2)]. \end{aligned} \tag{32}$$

By adding Eqs. (30)–(32) into Eq. (29) we can bring it to the generalized KH form of the stimulated Raman scattering,

$$\tilde{S}_{SRS}(\omega_1, \omega_2) = 4\pi N \sum_{g,g',e,f} P(g)|\mathscr{E}_1|^2|\mathscr{E}_2|^2|\mathscr{T}_{g'g}^{(2)}(\omega_1)|^2 \times \delta(\omega_1 - \omega_2 - \omega_{g'g}) - P(g)|\mathscr{E}_1|^2|\mathscr{E}_2|^2|\mathscr{T}_{g'g}^{(2)}(\omega_2)|^2 \times \delta(\omega_2 - \omega_1 - \omega_{g'g}) + P(g)|\mathscr{E}_2|^2|\mathscr{T}_{eg}^{(1)}|^2\,\delta(\omega_2 - \omega_{eg}) - P(g)|\mathscr{E}_2\mathscr{T}_{eg}^{(1)} + \tag{33}$$

In addition to terms corresponding to two interactions with the pump beam and two interactions with the probe beam. It contains higher-order terms in the field. Comparing the CTPL [Eq. (29)] and KH [Eq. (33)] expressions for the stimulated Raman scattering, we find that they only differ by six order terms in the optical field: $\tilde{S}_{SRS}(\omega_1, \omega_2) - S_{SRS}(\omega_1, \omega_2) = O(|\mathscr{E}_2|^2|\mathscr{E}_1|^4)$. The imaginary part in Eq. (29) is brought on the advanced Green's function across the loop in Eq. (33) and gives the Dirac delta function with the argument corresponding to specific molecular resonances.

In the form of Eq. (33), the SRS process can be interpreted as follows. The first term describes one photon depletion of the pump beam mode followed by the emission of a photon into the probe beam mode. The second term describes emission into the pump beam mode after a probe beam photon was annihilated. The two terms are of opposite sign and correspond to different resonances. In the degenerate case ($\omega_1 = \omega_2$) they exactly cancel each other. The remaining

terms describe perturbation in the probe beam linear absorption due to the pump beam. The pump beam, in a sense, catalyzes the molecular transitions from ground $|g\rangle$ to excited $|e\rangle$ since the number of photons in the pump beam mode remains unchanged [see diagrams (b) and (h) in Fig. 5].

We next turn to the TPA component of the pump-probe signal. Considering the diagrams (a) and (b) in Fig. 5 with switched the pump beam and the probe beam and using the diagrams transformation rules, we find the following identity:

$$\begin{aligned}[|\mathscr{T}_{fg}^{(2)}(\omega_2)|^2 &+\mathscr{T}_{fg}^{(2)}(\omega_2)\mathscr{T}_{fg}^{(2),\star}(\omega_1)]\frac{1}{\omega_2+\omega_1-\omega_{fg}-i\gamma}+[\mathscr{T}_{eg}^{(3)}(\omega_2\\ &+\omega_1,\omega_2)\mathscr{T}_{eg}^{(1),\star}\\ &+\mathscr{T}_{eg}^{(3)}(\omega_1\\ &+\omega_2,\omega_1)\mathscr{T}_{eg}^{(1),\star}]\\ &\times\frac{1}{\omega_2-\omega_{eg}-i\gamma}=0.\end{aligned} \tag{34}$$

In the above equation the first term is the absorption of the pump beam, and the last term is the emission of the pump beam. We will also need the high-order terms

$$4\pi N\,\mathrm{Im}\sum_{g,g',e,f}P(g)|\mathscr{E}_1|^4|\mathscr{E}_2|^2\frac{1}{\omega_2-\omega_{eg}-i\gamma}\times[\mathscr{T}_{eg}^{(3)}(\omega_2+\omega_1,\omega_2)\mathscr{T}_{eg}^{(3),\star}(\omega_2+\omega_1,\omega_2)+\mathscr{T}_{eg}^{(3)}(\omega_2+\omega_1,\omega_1)\mathscr{T}_{eg}^{(3),\star}(\omega_2+\omega_1,\omega_1)+\mathscr{T}_{eg}^{(3)}(\omega_2+\omega_1,\omega_2)\mathscr{T}_{eg}^{(3),\star}(\omega_2+\omega_1,\omega_1)+\mathscr{T}_{eg}^{(3)}(\tag{35}$$

Substituting Eqs. (31), (34), and (35) into Eq. (28) we again bring it to the generalized KH form

$$\tilde{S}_{TPA}(\omega_1,\omega_2)=-4\pi N\sum_{g,e,f}P(g)|\mathscr{E}_1|^2|\mathscr{E}_2|^2|\mathscr{T}_{fg}^{(2)}(\omega_1)+\mathscr{T}_{fg}^{(2)}(\omega_2)|^2\delta(\omega_2+\omega_1-\omega_{fg})+P(g)|\mathscr{E}_2\mathscr{T}_{eg}^{(1)}+|\mathscr{E}_1|^2\mathscr{E}_2\mathscr{T}_{eg}^{(3)}(\omega_2+\omega_1,\omega_2)+|\mathscr{E}_1|^2\mathscr{E}_2\mathscr{T}_{eg}^{(3)}(\omega_1+\omega_2,\omega_1)|^2\delta(\omega_2-\omega_{eg})-P(g)|\mathscr{E}_2| \tag{36}$$

Here the first two terms describe the absorption of the pump beam and the probe beam. The remaining terms represent the pump beam catalyzed change in the linear absorption of the probe beam. The KH form represents the two-photon absorption signal up to the fourth order in the optical field. Similar to SRS we have $\tilde{S}_{TPA}(\omega_1,\omega_2)-S_{TPA}(\omega_1,\omega_2)=O(|\mathscr{E}_2|^2|\mathscr{E}_1|^4)$.

Equations (27), (33), and (36) are equivalent to Eq. (26). The simple KH form in terms of modulus square of transition amplitudes is recovered for both TPA and SRS when the single-

photon transitions are off-resonant ($|\omega_2 - \omega_{eg}| \gg \eta$). Otherwise, in order to match that form, we must go beyond $\chi^{(3)}$; however we still use the same transition amplitudes which are the building blocks of $\chi^{(3)}$. A KH form of the signal is possible if we include six order terms which can be made negligible by keeping the fields sufficiently weak. The KH form can thus be used for numerical simulations provided we carefully adjust the field amplitudes $\mathcal{E}_1$ and $\mathcal{E}_2$, as is done experimentally.

VI. CONCLUSIONS

In this paper we have formulated heterodyne-detected (n + 1)-wave mixing signals using a quantum description of both the matter and the field. In this approach signals are defined as the change in intensity in the detected mode with and without the n incoming modes. As in the SC theory, these are expressed in terms of the nonlinear polarization induced by the incoming modes.

In the SC description of heterodyne-detected techniques the local oscillator serves as the detected mode. The present formalism does not require the local oscillator to be external to the material; the signal is viewed as a single (n + 1) photon process where all modes (the n incoming as well as the local oscillator) do interact with the material. Self-heterodyne detected signals such as a pump probe spectra arise naturally the same framework. All transitions (including the signal generation) are now stimulated, and spontaneous emission is neglected.

The CTPL provides a convenient diagrammatic tool for calculating the polarization for frequency-domain experiments. Rules for constructing and reading these diagrams were presented. It resolves certain conceptual ambiguities associated with double-sided Feynman diagrams. Contrary to latter, an arrow pointing to the right (left) always represents absorption (emission) irrespective on whether it is placed on the left or the right branch of the loop. The CTPL represents dynamics of a state in the Hilbert space which propagates forward (left branch) in time and then across the loop backward (right branch). This resolves the ambiguous role of the interaction at the observation time, which diagrammatically can be placed on either of the two branches. In the CTPL formalism this interaction has a definite interpretation as either photon emission or absorption.

For frequency-domain experiments the CTPL generally yields more compact expressions for the signal than the fully time-ordered double-sided Feynman diagrams [(n + 1) vs 2^n terms]. We have employed CTPL to derive an expression for the frequency-domain four-wave mixing signal $\mathbf{k}_c = -\mathbf{k}_1 + \mathbf{k}_2 + \mathbf{k}_3$. The CTPL is particularly useful when the signal is generated by highly nonclassical optical field and is not defined by the causal response function $\chi^{(3)}$. In this case dissecting the loop at the central line is not always justified since corresponding single or (and) three-photon optical transition amplitudes might vanish.

By treating both field and matter quantum mechanically, wave-mixing signals can be classified as either phase-sensitive or phase-insensitive type. The expressions for phase-sensitive signals contain a different number of creation and annihilation operators for at least one of the field modes. Phase-sensitive experiments are not possible with fields initially prepared in a Fock number state. The signal then vanishes identically. Such processes are only possible in the presence of a Fock-space-coherence of the field, e.g., when the field is in a coherent state. Such signals however, cannot be interpreted in terms of changes of photon occupation numbers as a difference of absorption and emission.

Expressions for phase-insensitive signals contain an equal number of creation and annihilation operators in each of the participating field modes. Such processes are possible even if the fields are initially prepared in number states and may therefore be interpreted more intuitively in

terms of photon occupation numbers. Each loop diagram can then be factorized into a product of two complex transition amplitudes represented by single-sided Feynman diagrams which only involve forward propagation. The signal can be interpreted as the difference between emission and absorption in the detected mode. As an example of a phase-insensitive signal we considered the pump probe technique composed of two-photon absorption and stimulated Raman scattering parts. By combining the CTPL with the *T* matrix formalism we approximate both signals by the generalized KH form. This shows that heterodyne detection selects only resonant components of the Im $\chi^{(n)}$ The KH form becomes an exact representation of the signal when single-photon transitions are off-resonant or at sufficiently low-field intensity when terms higher than $\sim|\mathcal{E}_1|^2|\mathcal{E}_2|^2$ make negligible contributions to the signal.

Acknowledgments

The support of the National Science Foundation (Grant No. CHE-0745892) and the National Institutes of Health (Grant No. GM59230) is gratefully acknowledged.

APPENDIX A: RULES FOR THE CTPL IN THE TIME DOMAIN

In this appendix we summarize the rules for the time-domain (TD) interpretation of the CTPL. Derivation of these rules may be found in Ref. [21].

TD1: in the time domain the loop represents the density operator. Its left branch stands for the ket, the right corresponds to the bra. Time runs from bottom to top on both branches.

TD2: each interaction with a field mode is represented by a wavy line on either the right (*R* operators) or the left (*L* operators).

TD3: the field is indicated by dressing the wavy lines with arrows, where an arrow pointing to the right represents the field annihilation operator $E(\mathbf{r}, t)$, which involves the term $e^{i(\mathbf{k}_j\cdot\mathbf{r}-\omega_j t)}$ [see Eq. (4)]. Conversely, an arrow pointing to the left corresponds to the field creation operator $E^{\dagger}(\mathbf{r}, t)$, being associated with $e^{-i(\mathbf{k}_j\cdot\mathbf{r}-\omega_j t)}$. This is made explicit by adding the wave vectors $\pm\mathbf{k}_j$ to the arrows.

TD4: within the RWA, each interaction with $E(\mathbf{r}, t)$ is accompanied by applying the operator $V^{\dagger}$, which leads to excitation of the state represented by the ket and de-excitation of the state represented by the bra, respectively. Arrows pointing “inwards” (i.e., pointing to the right on the ket and to the left on the bra) consequently cause absorption of a photon by exciting the system, whereas arrows pointing “outwards” (i.e., pointing to the left on the bra and to the right on the ket) represent de-exciting the system by photon emission.

TD5: the interaction at the observation time *t*, is fixed and is always the last. As a convention, it is chosen to occur from the left. This choice is arbitrary and does not affect the result.

TD6: interactions within each branch are time-ordered, but interactions on different branches are not. Each loop can be further decomposed into several fully time-ordered diagrams (double-sided Feynman diagrams). These can be generated from the loop by simply shifting the arrows along each branch, thus changing their position relative to the interactions on the other branch. Each of these relative positions then gives rise to a particular fully time-ordered diagram.

TD7: the overall sign of the correlation function is given by $(-1)^{N_R}$, where N_R stands for the number of interactions from the right.

TD8: diagrams representing $(n + 1)$-wave mixing acquire a common prefactor i^n.

APPENDIX B: RULES FOR THE CTPL IN THE FREQUENCY DOMAIN

In this appendix we summarize the rules for the frequency-domain (FD) interpretation of the CTPL. Derivation of these rules may be found in Ref. [21].

FD1: time runs along the loop clockwise from bottom left to bottom right.

FD2: each interaction with a field mode is represented by a wavy line.

FD3: the field is indicated by dressing the wavy lines with arrows, where an arrow pointing to the right represents the field annihilation operator $E(\mathbf{r}, t)$, which involves the factor $e^{i(\mathbf{k}_S\cdot\mathbf{r}-\omega_S t)}$. Conversely, an arrow pointing to the left corresponds to the field creation operator $E^{\dagger}(\mathbf{r}, t)$, being associated with $e^{-i(\mathbf{k}_S\cdot\mathbf{r}-\omega_S t)}$. This is made explicit by adding the wave vectors $\pm\mathbf{k}_s$ to the arrows.

FD4: within the RWA [Eq. (5)], each interaction with $E(\mathbf{r}, t)$ is accompanied by applying the operator $V^{\dagger}$, which leads to excitation of the material system. Arrows pointing to the right cause absorption of a photon by exciting the molecule, whereas arrows pointing to the left represent de-exciting the system by photon emission.

FD5: the interaction at the observation time t is fixed to be with the detected mode and is always the last. It is chosen to occur on the left branch of the loop. This choice is arbitrary and does not affect the result.

FD7: the loop translates into an alternating product of interactions (arrows) and periods of free evolutions (vertical solid lines) along the loop.

FD8: since the loop time goes clockwise along the loop, periods of free evolution on the left branch amount to propagating forward in real time (iG), whereas evolution on the right branch corresponds to backward propagation ($-iG^{\dagger}$).

FD9: the frequency arguments of the various propagators are cumulative, i.e., they are given by the sum of all "earlier" interactions along the loop. Additionally, the ground-state frequency ω_g is added to all arguments of the propagators.

FD10: a diagram representing $n + 1$ mixing caries the prefactor $i^n(-1^{N_R})$ (N_R is the number of interactions from the right).

APPENDIX C: THE SCATTERING T MATRIX ELEMENTS

In scattering theory the T matrix is given by $T = V + VG(E)V$. By working in the joint matter and field space we only need this definition where E is the initial energy. However, we shall define a scattering matrix in the matter space alone $\mathscr{T}$. Changes in the numbers of photons can then be included by varying the argument of the Green's function since the energy of the system alone is not conserved. This will require to define different $\mathscr{T}$ matrix for each order as a series of multiphoton transition amplitudes (TAs) as

$$\begin{aligned}\mathscr{T} &= \mathscr{T}^{(1)} + \mathscr{T}^{(2)}(\omega) + \mathscr{T}^{(3)}(\omega' \pm \omega, \omega) + \cdots \\ &= V' + V'G(\omega+\omega_g)V' + V'G(\omega' \pm \omega + \omega_g) \times V'G(\omega+\omega_g)V' + \cdots,\end{aligned} \tag{C1}$$

where the dipole moment operator is portioned as $V' = V + V^{\dagger}$. The superscript indicates the order (number of interactions with V) of each term. For the three-level system initially in its ground state shown in Fig. 1 we obtain the following matrix elements.

Single-photon transition will need

$$\mathscr{T}_{eg}^{(1)} = \left\langle e|V^{\dagger}|g\right\rangle = \mu_{eg}. \tag{C2}$$

Two-photon transitions are described by

$$T_{g'g}^{(2)}(\omega) = \left\langle g'|VG(\omega+\omega_g)V^{\dagger}|g\right\rangle = \frac{\mu_{g'e}\mu_{eg}}{\omega-\omega_{eg}+i\gamma}, \tag{C3}$$

$$\mathscr{T}_{fg}^{(2)}(\omega) = \left\langle f|V^{\dagger}G(\omega+\omega_g)V^{\dagger}|g\right\rangle = \frac{\mu_{fe}\mu_{eg}}{\omega-\omega_{eg}+i\gamma}. \tag{C4}$$

Three-photon transitions need

$$\begin{aligned}\mathscr{T}_{eg}^{(3)}(\omega'-\omega,\omega) &= \left\langle e|V^{\dagger}G(\omega'-\omega+\omega_g)VG(\omega+\omega_g)V^{\dagger}|g\right\rangle \\ &= \frac{\mu_{eg'}\mu_{g'e}^{\star}\mu_{eg}}{(\omega'-\omega-\omega_{g'g}+i\gamma)(\omega-\omega_{eg}+i\gamma)},\end{aligned} \tag{C5}$$

$$\begin{aligned}\mathscr{T}_{eg}^{(3)}(\omega'+\omega,\omega) &= \left\langle e|VG(\omega'+\omega+\omega_g)V^{\dagger}G(\omega+\omega_g)V^{\dagger}|g\right\rangle \\ &= \frac{\mu_{eg}^{\star}\mu_{fe}\mu_{eg}}{(\omega'+\omega-\omega_{fg}+i\gamma)(\omega-\omega_{eg}+i\gamma)}.\end{aligned} \tag{C6}$$

The *T* matrix elements can be illustrated by single-sided Feynman diagrams. The diagrams relevant for the pump-probe signal are shown in Fig. 4.

References

1. Bloembergen, N. Nonlinear Optics. 4th ed.. Singapore: World Scientific; 1996.
2. Bloembergen N. Am. J. Phys 1967;35:989.
3. Barron LD. J. Phys. B 1970;3:1558.
4. Denk W, Strickler JH, Webb WW. Science 1990;248:73. [PubMed: 2321027]
5. Peticolas WL, Goldsborough JP, Reickhoff KE. Phys. Rev. Lett 1963;10:43.
6. Freudiger CW, Min W, Saar BG, Lu S, Holtom GR, He C, Tsai JC, Kang JX, Xie XS. Science 2008;322:1857. [PubMed: 19095943]
7. Albota M, et al. Science 1998;281:1653. [PubMed: 9733507]
8. Mallick B, Lakshmanna A, Radhalakshmi V, Umapathy S. Curr. Sci 2008;95:1551.
9. Laimgruber S, Schachenmayr H, Schmidt B, Zinth W, Gilch P. Appl. Phys. B: Lasers Opt 2006;85:557.
10. Yoshizawa M, Kurosawa M. Phys. Rev. A 1999;61:013808.
11. Kukura P, David W, Mathies RA. Annu. Rev. Phys. Chem 2007;58:461. [PubMed: 17105414]
12. Scully, MO.; Zubairy, MS. Quantum Optics. Cambridge: Cambridge University Press; 1997.
13. Shen, YR. The Principles of Nonlinear Optics. New York: Wiley & Sons; 2002.
14. Mukamel, S. Principles of Nonlinear Optical Spectroscopy. USA: Oxford University Press; 1995.
15. Andrews, DL.; Allcock, P. Optical Harmonics in Molecular Systems. Weinheim: Wiley-VCH; 2002.
16. Landauer R. IBM J. Res. Dev 1957;1:223.
17. Harbola U, Mukamel S. Phys. Rep 2008;465:191.

18. Glauber, RJ. Quantum Theory of Optical Coherence. Berlin: Wiley-VCH Verlag; 2007.
19. Berman PR, Boyd RW, Milonni PW. Phys. Rev. A 2006;74:053816.
20. Bialynicki-Birula I, Sowinski T. Phys. Rev. A 2007;76:062106.
21. Marx CA, Harbola U, Mukamel S. Phys. Rev. A 2008;77:022110.
22. Schwinger J. J. Math. Phys 1961;2:407.
23. Keldysh LV. Sov. Phys. J 1965;20:1018.
24. Mukamel S. Phys. Rev. A 2008;77:023801.
25. Cohen AE, Mukamel S. Phys. Rev. Lett 2003;91:233202. [PubMed: 14683180]
26. Mukamel S. Phys. Rev. E 2003;68:021111.
27. Keldysh LV. Sov. Phys. JETP 1965;20:1018.
28. Rammer, J. Quantum Field Theory of Nonequilibrium States. Cambridge: Cambridge University Press; 2007.
29. Negele, JW.; Orland, H. Quantum Many-Particle Systems. Westview Press; 1998.
30. Gorkov, LP.; Gor'kov, LP.; Dzyaloshinski, IE.; Silverman, RA. Methods of Quantum Field Theory in Statistical Physics. Englewood Cliffs, NJ: Prentice Hall; 1975. joint author
31. Mills, R. Propagators for Many-particle Systems. New York: Gordon and Breach; 1969.

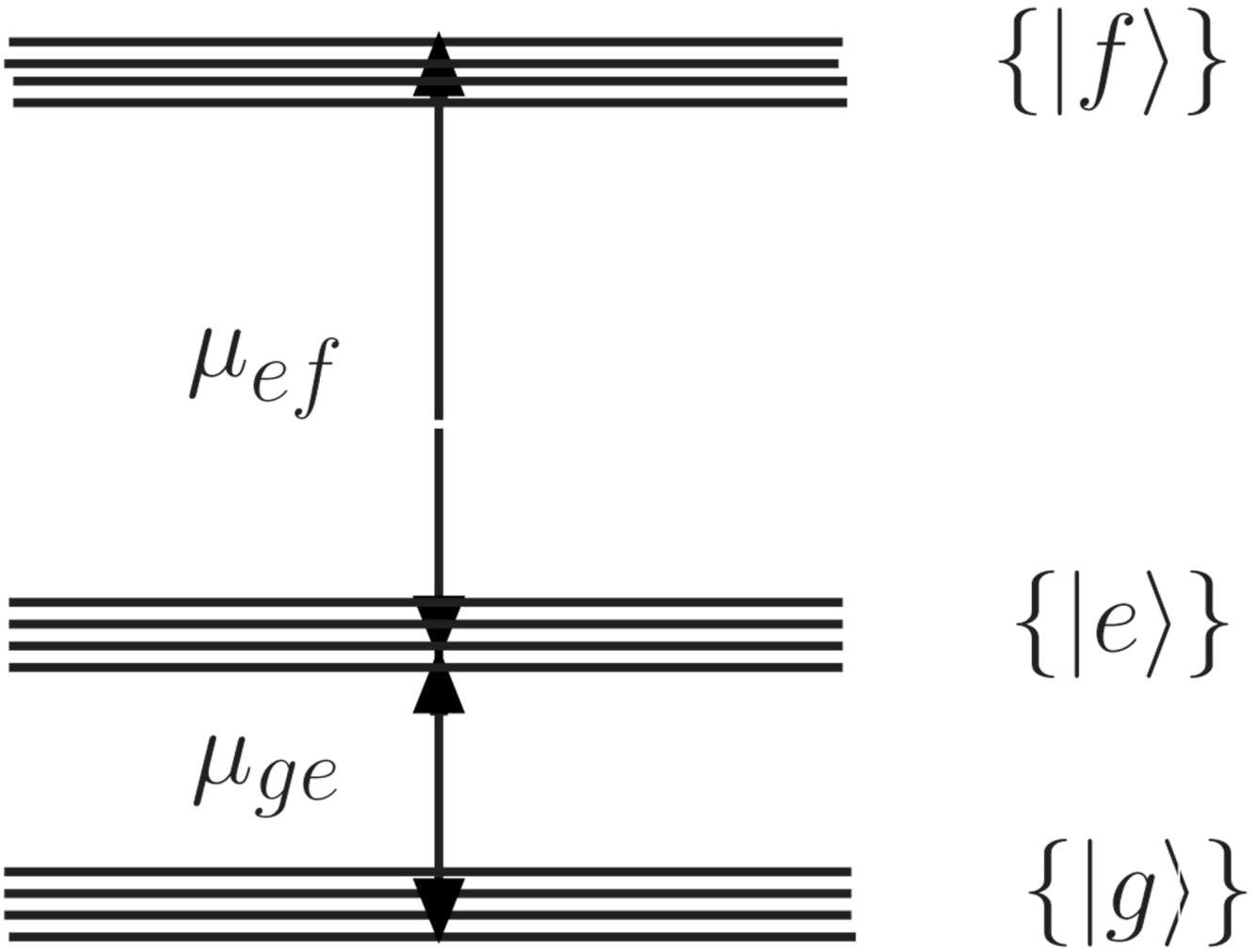

FIG. 1.
The three-band (ladder) model system and its transition dipoles.

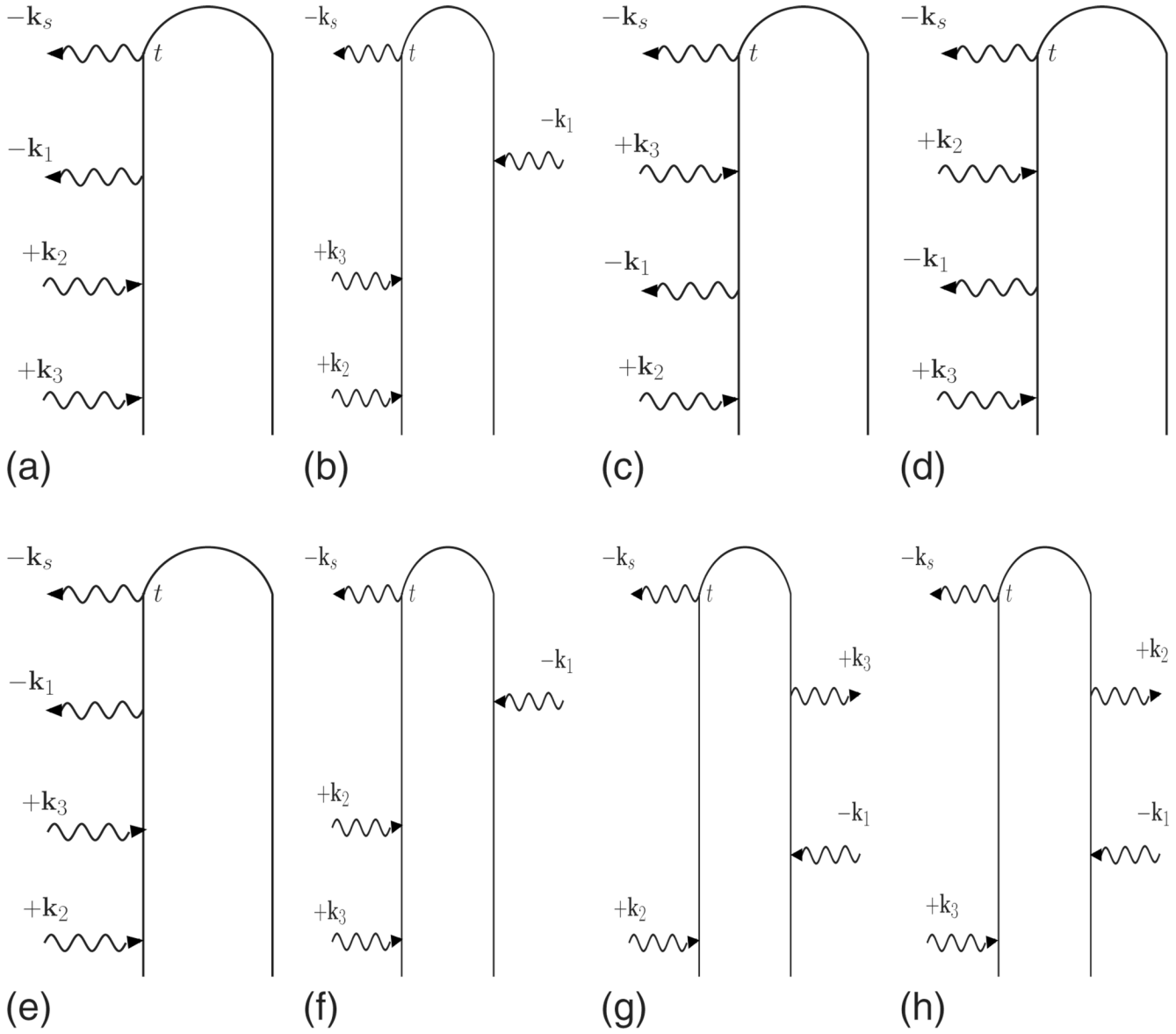

FIG. 2.

CTPL representation of the heterodyne detected $\mathbf{k}_c = -\mathbf{k}_1 + \mathbf{k}_2 + \mathbf{k}_3$ signal. Diagrams (a)–(d) represent two-photon absorption and the diagrams (e)–(h) represent the stimulated Raman scattering.

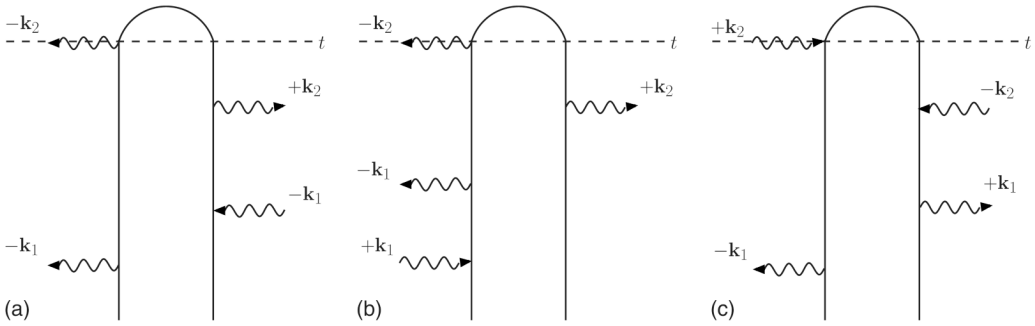

FIG. 3.

CTPL diagrams for the processes (a) ($|n_1, n_2\rangle \rightarrow |n_1 + 1, n_2 + 1\rangle$), (b) ($|n_1, n_2\rangle \rightarrow |n_1, n_2 + 1\rangle$), and (c) ($|n_1, n_2\rangle \rightarrow |n_1 + 1, n_2 - 1\rangle$). These correspond to the lowest-order contributions to each of the processes given in terms of four-point correlation functions. These diagrams violate the RWA since they involve de-exciting the material system from its ground state.

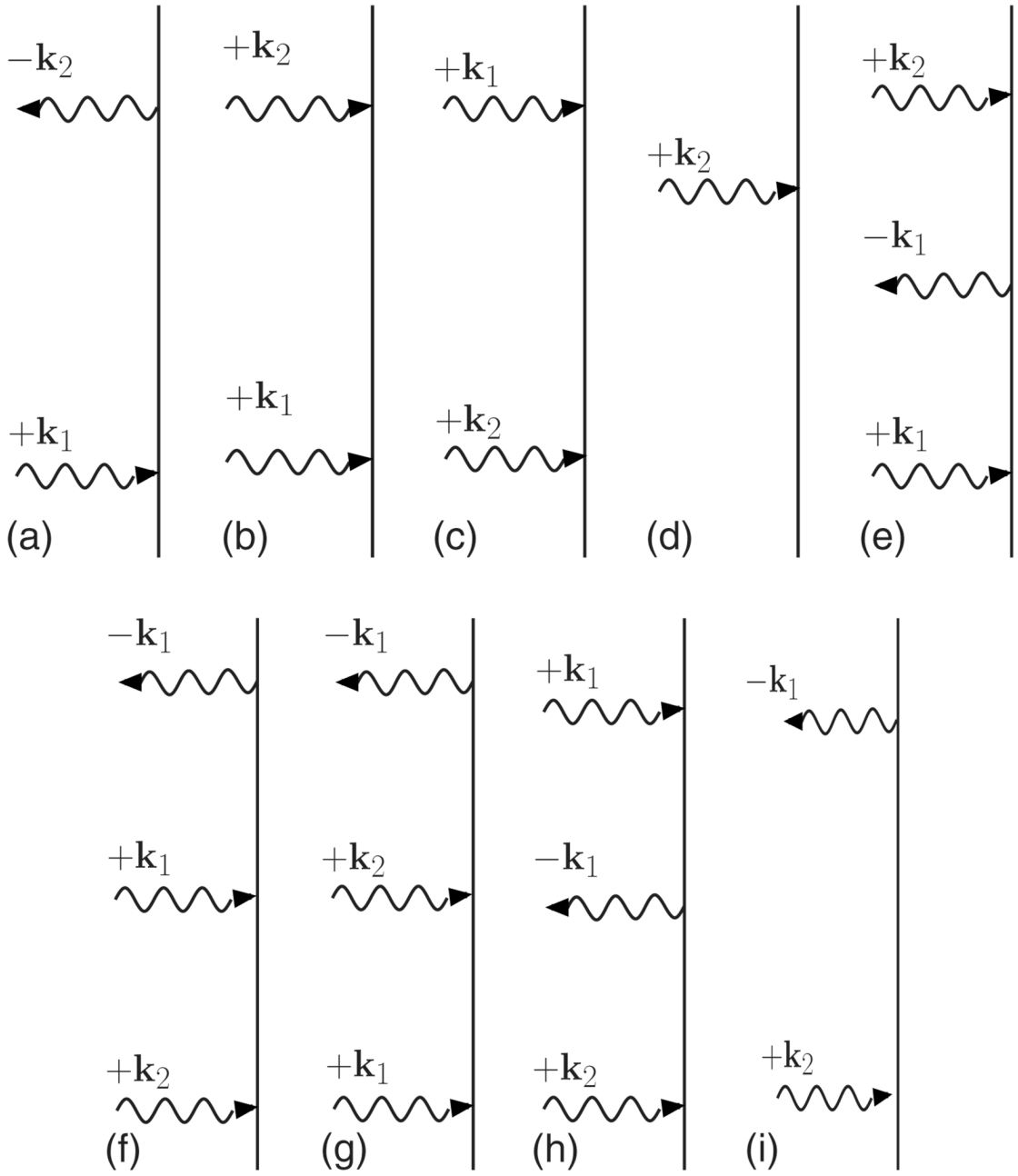

FIG. 4.

Single-sided Feynman diagrams representing the amplitudes of processes of types (i)–(iv). The possible realizations (pathways) of the three processes are classified with respect to the number of interactions (=order). Time now runs from bottom to top. Process (ii) is realized by two second-order pathways, shown in panels (b) and (c). Process (iii) can be realized by a first order pathway [panel (d)] or by third-order pathways [panels (e)–(h)]. Processes (i) and (iv) are given by second-order pathways illustrated in panel (a) and (k).

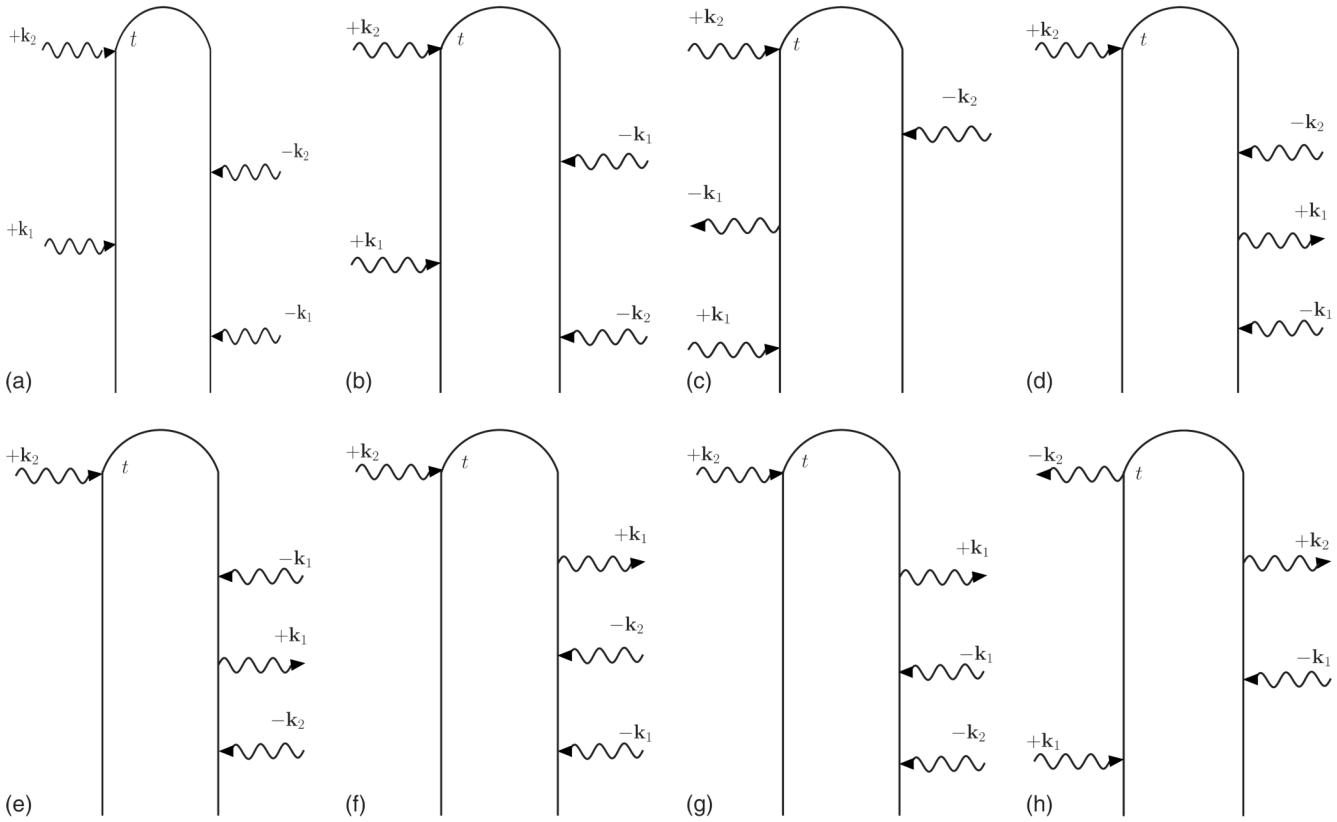

FIG. 5.

The eight CTPL diagrams for the pump-probe signal. These can be grouped into three processes according to the state of the field at the observation time, t, into three processes: (a) and (b) $|n_1, n_2\rangle \rightarrow |n_1 - 1, n_2 - 1\rangle$, (c)–(g) $|n_1, n_2| \rightarrow |n_1, n_2 - 1\rangle$, and (h) $|n_1, n_2\rangle \rightarrow |n_1 - 1, n_2 + 1\rangle$.

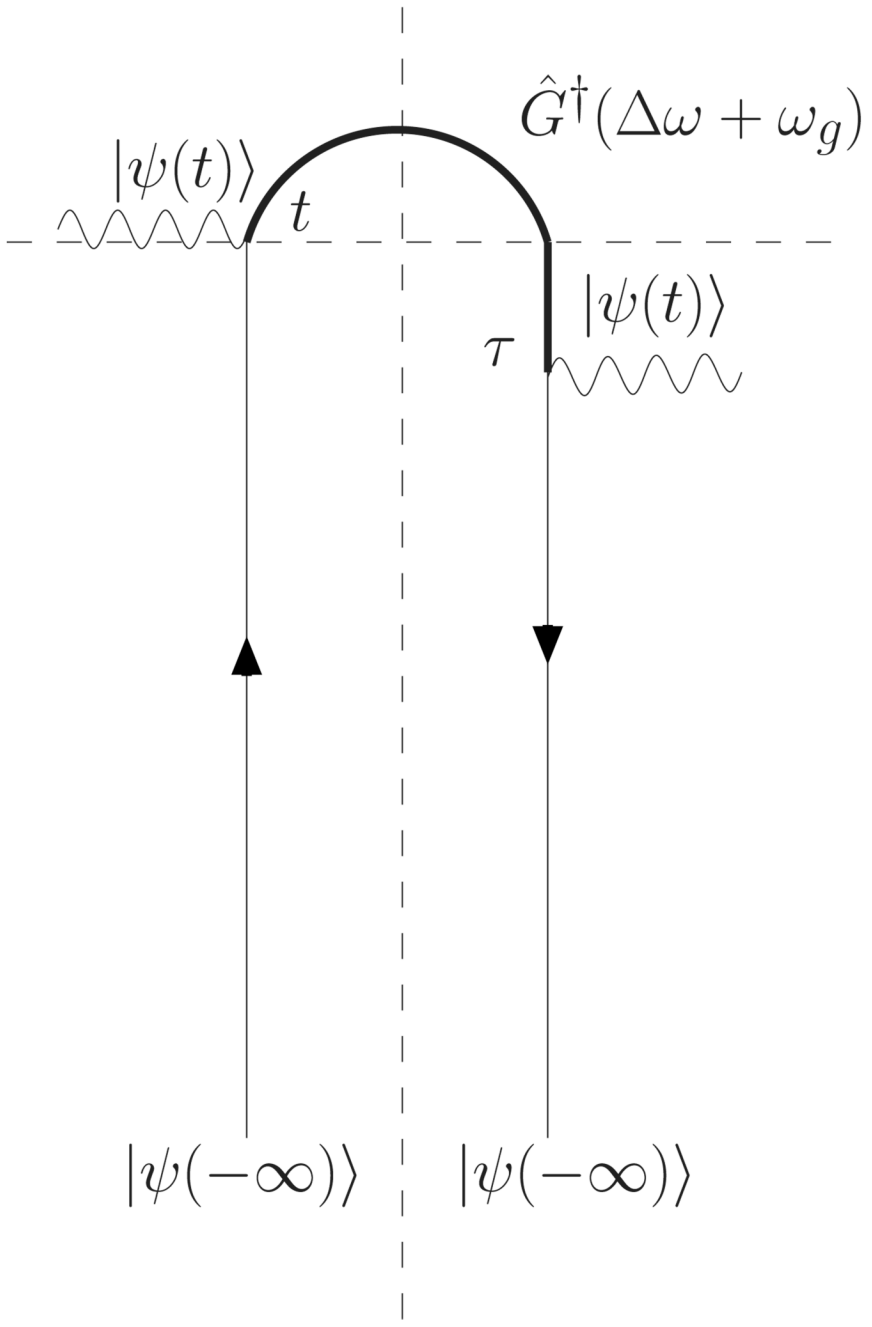

FIG. 6.

By dissecting the loop along its center line it factorizes into two single-sided Feynman diagrams. This is possible since the system remains in the same state $|\psi(t)\rangle$ between the topmost interaction on the two branches which occur, respectively, at times t and τ. The advanced propagator $G^{\dagger}(\Delta\omega + \omega_g)$, representing backward propagation from t to τ, joins the two.